

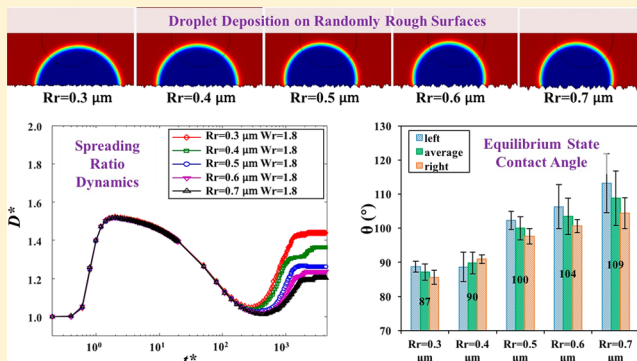
Computational Study of Single Droplet Deposition on Randomly Rough Surfaces: Surface Morphological Effect on Droplet Impact Dynamics

Jie Xiao,*[†]^{ID} Fei Pan,[†] Hongtao Xia,[†] Siyu Zou,[†] Hui Zhang,[†] Oluwafemi Ayodele George,[†] Fei Zhou,[†] and Yinlun Huang[‡]^{ID}

[†]Suzhou Key Laboratory of Green Chemical Engineering, School of Chemical and Environmental Engineering, College of Chemistry, Chemical Engineering and Materials Science, Soochow University, Suzhou 215123, China

[‡]Department of Chemical Engineering and Materials Science, Wayne State University, Detroit, Michigan 48202, United States

ABSTRACT: Tremendous efforts have been devoted to the modeling of droplet deposition on smooth and patterned surfaces with ordered structures. However, systematic work focusing on randomly rough surfaces, which are the most common bare substrate surfaces, can be hardly identified. A phase field modeling method together with a unique analysis approach has been developed in this work to characterize single droplet deposition on randomly rough surfaces. It is interesting to observe that the droplet shape evolves quite differently on a randomly rough surface, as compared to a patterned surface, even if two surfaces have the same roughness. Parametric studies have been carried out to explore how the morphological metrics of randomly rough surfaces, which include the Wenzel roughness parameter (W_r) and the root-mean-square roughness (R_r), can affect droplet impact dynamics. The quantitative relationships derived from this study can eventually shed light on droplet shape on-aim control during the deposition process, which is of great practical importance in many applications.



1. INTRODUCTION

Paint-based surface coatings are conventionally manufactured through two consecutive operational steps, i.e., spray and curing.¹ In operation, coating formation involves a continuous deposition of a large quantity of small droplets on a substrate, which is followed by solvent evaporation and thermal curing of the wet thin film.^{2,3} It has been found experimentally that the initial morphology of the substrate does affect the final coating morphology, since some textures of the coating on a rough surface do not appear in the coating on a smooth substrate such as glasses.⁴ Quantitative understanding of how the bare substrate morphology can affect surface texture evolution throughout the coating formation process is an extremely challenging task but of great importance to coating quality control. Exploration of the dynamics of the single droplet deposition becomes a necessary first step toward a comprehensive understanding of the complete coating formation process.

Tremendous experimental and modeling efforts can be identified to quantify the equilibrium contact angle of a droplet deposited on smooth and rough surfaces.^{5–9} The objective is mainly to design functional surfaces with desired hydrophobicity based on the quantitative correlation between surface properties (i.e., chemistry and morphology) and equilibrium contact angle.^{5,6,10–14}

Understanding single droplet deposition is much more challenging since it is a multistage process that involves initial spreading, retraction and rebound, and relaxation to the final equilibrium state.¹⁵ The impact dynamics are inevitably influenced by multiple factors simultaneously, which can generally be divided into two groups, i.e., materials properties and operational conditions. The properties of a liquid droplet include its density, viscosity, and surface tension, while the properties of a substrate include the surface morphology and chemistry. The operational conditions that can be manipulated refer to the droplet size, impact velocity, surface temperature, etc. Although it is extremely difficult to derive quantitative and comprehensive correlations between the above-listed factors and deposition dynamics, continuous efforts with specific focuses have been carried out to improve our understanding of this complex process. Two groups of models can be identified so far: analytical models and numerical ones. Three independent dimensionless numbers have been extensively utilized in analytical models to characterize the droplet deposition process, which are the Weber number (We), the Reynolds number (Re),

Received: January 26, 2018

Revised: April 21, 2018

Accepted: May 11, 2018

Published: May 11, 2018

and the contact angle (θ). Scheller and Bousfield were interested in correlating them with the maximum spreading radius of a Newtonian droplet.¹⁶ In addition to the maximum spreading radius, Mao et al. investigated the tendency of rebound.¹⁷ Dong et al. carried out comprehensive experiments on inkjet drop impaction on surfaces.¹⁸ Experimental results on maximum spreading ratio were compared with those predicted by most existing analytical models. Gao and Li derived theoretical equations based on energy conservation to quantify spread diameter during the recoiling stage.¹⁹ Numerical models are promising alternatives to investigate droplet deposition. Compared with analytical ones, numerical models use fewer assumptions and promote a more reliable prediction. Additional information can be derived from simulation results, since droplet shape evolution throughout the complete deposition process can be reproduced.^{19–21}

Most existing efforts, however, focused on the study of droplet deposition on smooth surfaces. Usually, the process was investigated over a wide range of impact velocities, droplet diameters, and surface contact angles. Systematic study of the surface morphological effects on droplet impact dynamics can be hardly identified, which is especially true for systems with randomly rough surfaces, i.e., the most common bare substrate surfaces. Li et al. (2013) derived a theoretical model for maximum spreading factor on a patterned surface with ordered microposts.²² Lattice Boltzmann models were developed to numerically simulate the spreading of droplets on textured surfaces.^{22–25} It remains unclear how the droplet impact behavior on structured surfaces can sufficiently resemble that on randomly rough surfaces. David and Neumann modeled the contact angle hysteresis on randomly rough surfaces.²⁶ Through simulating a vertical plate dipped into a pool of liquid, they described the wetting behavior of solid surfaces by liquids. It is, however, not a droplet impact study. Yuan and Zhang simulated droplet impact on rough surfaces using the lattice Boltzmann method.²⁷ They focused on the bouncing behavior of a droplet on superhydrophobic surfaces. Very limited experimental work can be identified.^{28,29} The understanding of droplet impact behavior on randomly rough surfaces has to be improved. Note that when a droplet impacts on a surface, it may stick, recoil, rebound, or splash. Different types of splash are possible. The situation becomes more complicated when the surface temperature is high,³⁰ which may lead to the Leidenfrost effect. Some regime maps were reported to predict droplet impact behavior based on the Weber number and the surface temperature.^{31,32} In this work, however, the phenomenon to be investigated is paint droplet deposition for wet film formation at room temperature. Thus, there is no heat exchange between the surface and the droplet.

In this work, a numerical model based on the phase field method was developed to characterize the complete multistage process of droplet deposition on randomly rough surfaces. Comparisons between impact dynamics on ordered surfaces and those on randomly rough surfaces demonstrated the need for the current study. Systematic analysis is then conducted to explore how the carefully designed surface morphological metrics can affect droplet impact behavior.

2. MATHEMATICAL MODELING AND SIMULATION METHOD

As stated in the last section, investigation of the surface morphological effects on droplet impact dynamics has attracted great interest. However, droplet impact on randomly rough

surfaces can be hardly identified. As will be discussed later on, this work indeed shows a clear distinction in droplet impact dynamics between the commonly investigated smooth and regular surfaces as compared to the randomly rough surfaces. Since the majority of the real surfaces are neither smooth nor regular, a systematic understanding of droplet impact on randomly rough surfaces would be of great practical significance. Detailed numerical simulations have been carried out to help interpret and understand droplet impact on a randomly rough surface, focusing on tracking droplet shape evolution, i.e., the dynamics of the droplet–air interface.

The following assumptions have been made to facilitate modeling and simulation. The initial temperature is 20 °C, and it does not change throughout the process. Thus, the droplet and the surface have the same temperature, i.e., 20 °C. Heat exchange between the droplet and the substrate is not a concern in this work. The current study is restricted to the 2D system shown in Figure 1, which is a conventionally adopted scheme for droplet impact studies and will build a basis toward a time-consuming 3D investigation.

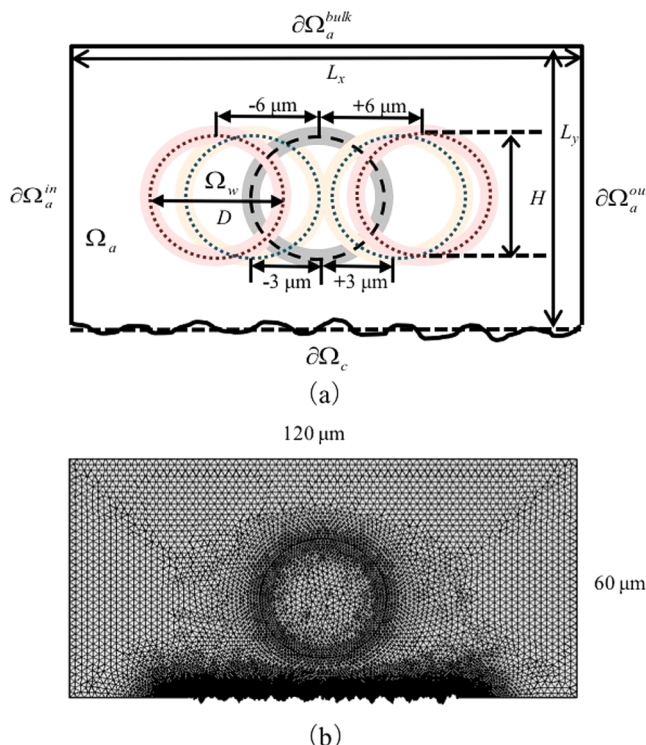


Figure 1. Simulation system: (a) schematic diagram of the computational domain showing five different droplet locations, and (b) the mesh of the domain with very fine grids on and adjacent to the rough surface for capturing droplet impact dynamics.

2.1. Governing Equations. In this work, the interfaces are tracked by the phase-field method.³³ The incompressible liquid–air flow of mass and momentum are represented by the modified Navier–Stokes conservation equations,

$$\nabla \cdot \vec{V} = 0 \quad (1)$$

$$\rho \frac{\partial \vec{V}}{\partial t} + \rho(\vec{V} \cdot \nabla) \vec{V} = \nabla \cdot (-p \vec{I} + \mu(\nabla \vec{V} + \nabla \vec{V}^T)) + \mathbf{F} \quad (2)$$

where \vec{V} is the velocity vector (m/s) shared between the two phases, p is the pressure (Pa), and F is the volume force (N/m³). It accounts for both the interfacial body force, which is used in the phase-field model to include the effect of surface tension within the diffusive interface domain, as well as the gravitational force due to the weight of the falling droplet.

$$\mathbf{F} = G\nabla\phi + \rho\vec{g} \quad (3)$$

where \vec{g} is the gravity vector (m/s²), G is the chemical potential (J/m³), and ϕ is a dimensionless phase-field parameter.

The Cahn–Hilliard equation governs the evolution of the phase field parameter. The interface between the two phases is tracked by the solution of a continuity equation,

$$\frac{\partial\phi}{\partial t} + \vec{V}\cdot\nabla\phi = \nabla\cdot\beta\nabla G \quad (4)$$

where β is the mobility (m³/s/kg) that determines the time scale of the Cahn–Hilliard diffusion. Using eq 5, an exact numerical conservation of the integral of ϕ can be obtained. The dimensionless phase field parameter, ϕ , always assumes a value of 1 or -1 in each fluid except at the phase boundary where it is related to the volume fraction as,

$$\alpha_k = \begin{cases} \min\left[\left(\max\left(\frac{1+\phi}{2}, 0\right)\right), 1\right], \\ \quad k = 1 \text{ (i. e., phase 1)} \\ 1 - \min\left[\left(\max\left(\frac{1+\phi}{2}, 0\right)\right), 1\right], \\ \quad k = 2 \text{ (i. e., phase 2)} \end{cases} \quad (5)$$

In order to compute the chemical potential, the mixing energy assumes the Ginzburg–Landau form, i.e.,

$$E_{mix}(\phi, \nabla\phi) = \frac{1}{2}\lambda|\nabla\phi|^2 + \frac{\lambda}{4\varepsilon^2}(\phi^2 - 1)^2 \quad (6)$$

The mixing energy density, λ (N), and the interface thickness, ε (m), are related to the surface tension, σ (N/m), between the liquid and the surrounding gas by,

$$\sigma = \frac{2\sqrt{2}}{3}\frac{\lambda}{\varepsilon} \quad (7)$$

Combination of eqs 6 and 7 allows the calculation of the chemical potential,

$$G = \frac{\partial E_{mix}}{\partial\phi} - \nabla\cdot\frac{\partial E_{mix}}{\partial\nabla\phi} = \lambda\left[-\nabla^2\phi + \frac{\phi(\phi^2 - 1)^2}{\varepsilon^2}\right] \quad (8)$$

2.2. Generation and Characterization of Randomly Rough Surfaces. The randomly rough surfaces in this work are self-affine 2D profiles modeled by the Weierstrass–Mandelbrot (W-M) function (see Figure 1(b)).³⁴ The W-M function has been conventionally used to simulate rough surfaces, including the stainless steel plates.³⁵ The algorithm allowed us to generate surfaces with different structural features but the same roughness. Effects of two types of roughness on droplet impact dynamics were explored in this work, which are listed below.

Wenzel roughness, W_r , expresses the ratio between the actual and projected solid surface area.⁵ It is also called Wenzel roughness ratio.

The root-mean-square roughness (R_r) defines the root-mean-square average of the roughness profile, i.e.,

$$R_r = \sqrt{\frac{\sum_{i=1}^n (h_i - \bar{h})^2}{n}} \quad (9)$$

where \bar{h} is the mean height of all n data points.

The adopted W-M function³⁴ allowed us to set the root-mean-square roughness (i.e., R_r). The Wenzel roughness, W_r , could then be manipulated by adjusting the value of the fractal dimension. Surfaces investigated in this work have a fractal dimension value between 1.040 and 1.634. It can be observed that with a constant W_r , R_r can be increased through the decrease of the fractal dimension, i.e., with the loss of details indicating the decrease of the number of break points between edges. With a constant R_r , increasing W_r can lead to the increase of the fractal dimension, i.e., the higher number of details (break points between edges).

2.3. Initial and Boundary Conditions and Model Implementation. The two-phase flow conservation equations were solved in the space shown in Figure 1(a), which contains two domains, i.e., the air domain Ω_a and the liquid domain Ω_w . Air inlet and outlet conditions were applied to $\partial\Omega_a^{in}$ and $\partial\Omega_a^{out}$, respectively. This model thus enabled us to investigate droplet impact under specified external air flow conditions, though in this work the inlet velocity of air from $\partial\Omega_a^{in}$ was zero. The top surface $\partial\Omega_a^{bulk}$ was open to the bulk air. The randomly rough surface $\partial\Omega_c$ was set as a wetted wall with a contact angle of θ_0 .

For a phase field method, the initial velocity of the droplet has to be zero. In order to speed up the droplet to reach a prespecified impact velocity, a temporary external force was applied vertically to the droplet that was initially placed at a certain distance away from the rough surface. The magnitude and duration of this artificial force could be readily calculated. It should be pointed out that this external force was removed once the droplet touched the surface. To better capture the morphological effect of the randomly rough surface on droplet impact dynamics, for each randomly rough surface, a total of five simulations were conducted with five different droplet impact locations, i.e., central position, 3 and 6 μm to the left side, and 3 and 6 μm to the right side (see Figure 1(a)).

All the model equations in this study were numerically solved by COMSOL Multiphysics.³⁶ All the representative Navier–Stokes equations describing the physical attributes of the model were transformed into their weak forms, followed by numerical analyses carried out using a finite element method. The entire chamber geometry was meshed using triangular cells and the total number of cells was about 74,000 (see Figure 1(b)). Finer meshes were used for the rough surface to better capture droplet dynamics on the surface. The minimum element size for the rough surfaces is 0.09 μm . The minimum element size for the remaining domain is around three times larger, i.e., 0.25 μm .

2.4. Quantification of Droplet Impact. Toward quantitative analyses on droplet impact dynamics, the following dimensionless variables are defined:

$$\begin{cases} D^* = \frac{D}{D_0} \\ H^* = \frac{H}{D_0} \\ t^* = \frac{tV_0}{D_0} \end{cases} \quad (10)$$

Table 1. Droplet and Surface Properties

Cases	Diameter (μm)	Density (kg/m^3)	Viscosity (mPa·s)	Surface tension (N/m)	Contact angle	Impact velocity (m/s)	Temperature (°C)
Validation case 1 (Gunjal et al., 2005) ¹⁹	2500	1000	1	0.073	110°	0.3	NA
Validation case 2 (Dong et al., 2007) ¹⁵	40.9	1000	0.893	0.072	88°	2.21	25
Investigated cases	30	1140	150	0.02	80°	15	20

$$\begin{cases} R_e = \frac{\rho_w V_0 D_0}{\mu_w} \\ W_e = \frac{\rho_w V_0^2 D_0}{\sigma} \end{cases} \quad (11)$$

where D_0 is the droplet initial diameter (m), t is time (s), V_0 is the velocity of impact (m/s), and D and H are, respectively, the furthest horizontal and vertical distances between droplet surface points. Their values evolve during the impact process. The Reynolds number, Re , characterizes the ratio between the inertia force and the viscous force while the Weber number, We , characterizes the ratio between the inertial force and the surface tension force.

Force evolution throughout the deposition process can help us understand droplet shape evolution. The shear stress at the liquid–gas interface and the shear stress exerted by the fluid on the rough surface¹⁹ can be quantified by multiplying local fluid viscosity by local shear rate. Average shear stresses can be further obtained through carrying out area average (over the liquid–gas interface region) and line average (over the rough surface profile) in 2D respectively.

Tracking evolution of the triple-phase (solid–liquid–gas) contact line can reveal the wetting behavior of droplets on different rough surfaces. In a 2D system, a triple phase contact line becomes multiple contact points. The position of triple-phase contact points can be identified as the intersection points of the rough surface profile and the liquid–gas interface profile. The liquid–gas interface profile is taken as the contour line indicating locations where the volume fraction of liquid is 0.5.

Furthermore, the equilibrium state of droplets after the impact is quantified by the contact area and the contact angle. In a 2D system, the dimensionless liquid–solid contact area is defined as

$$A^* = \frac{l}{D_0} \quad (12)$$

where l is the length of the liquid–solid contact line. The surface is randomly rough, which offers two apparent contact angles in a 2D system. The equilibrium contact angle is then defined as

$$\theta = \frac{\theta_1 + \theta_2}{2} \quad (13)$$

where θ_1 and θ_2 are left and right contact angles, respectively. Xiao and Chaudhuri developed a detailed method to determine the apparent contact angles based on the shape of the droplet on a rough surface.³³ For each randomly rough surface, five simulations with different droplet impact locations are conducted. Droplet impact dynamics (i.e., D^* and H^* as a function of t^*) are then plotted using average values from five simulation runs. Average values and standard deviations of the equilibrium contact area and the equilibrium contact angle can also be obtained.

2.5. Model Validation. To verify the droplet impact model, numerical studies were conducted to investigate the impact behavior of both millimeter scale and micrometer scale droplets on surfaces. In Case 1, a 2.5 mm droplet impacts on a flat Teflon surface with an impact velocity of 0.3 m/s and a contact angle of 110° (see Table 1). The Weber and Reynolds numbers are 3.12 and 750, respectively. These data correspond to the experimental conditions used in Gunjal et al. (2005).¹⁹ The same trend between the model prediction and experimental data can be observed (see Figure 2(a)). When compared with the volume of fluid (VOF) approach by Gunjal et al. (2005),¹⁹ the current model performed slightly better in capturing oscillation magnitude, especially for the later stage of impact. Figure 2(a)

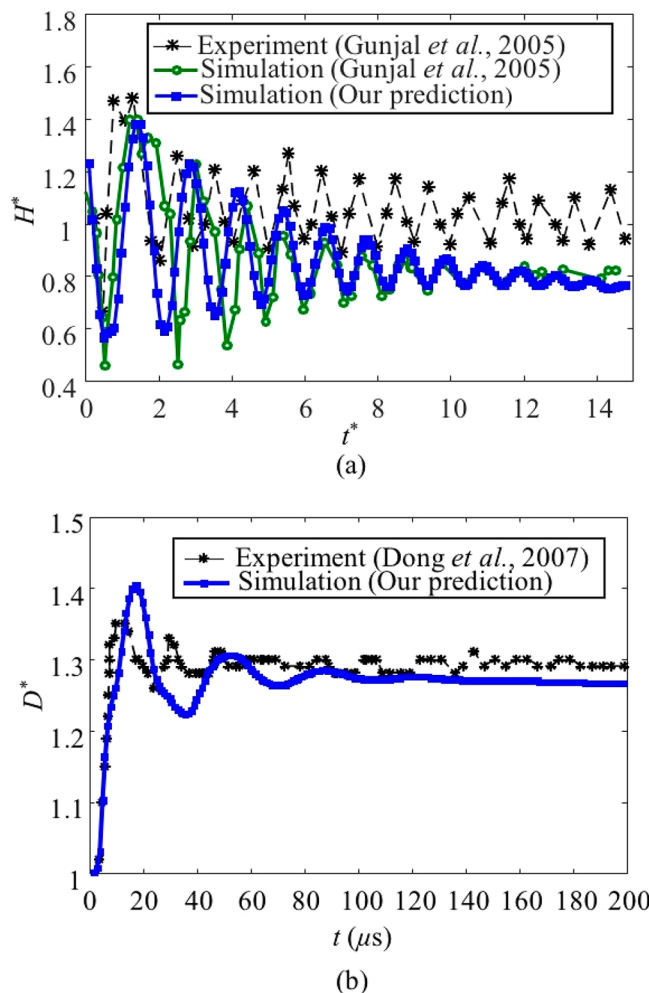


Figure 2. Comparison between experimental data^{15,19} and simulation results: (a) evolution of the dimensionless height as a function of the dimensionless time for a 2.5 mm droplet, and (b) evolution of the spreading ratio as a function of time for a 40.9 μm droplet. Droplet and surface properties for both cases are listed in Table 1.

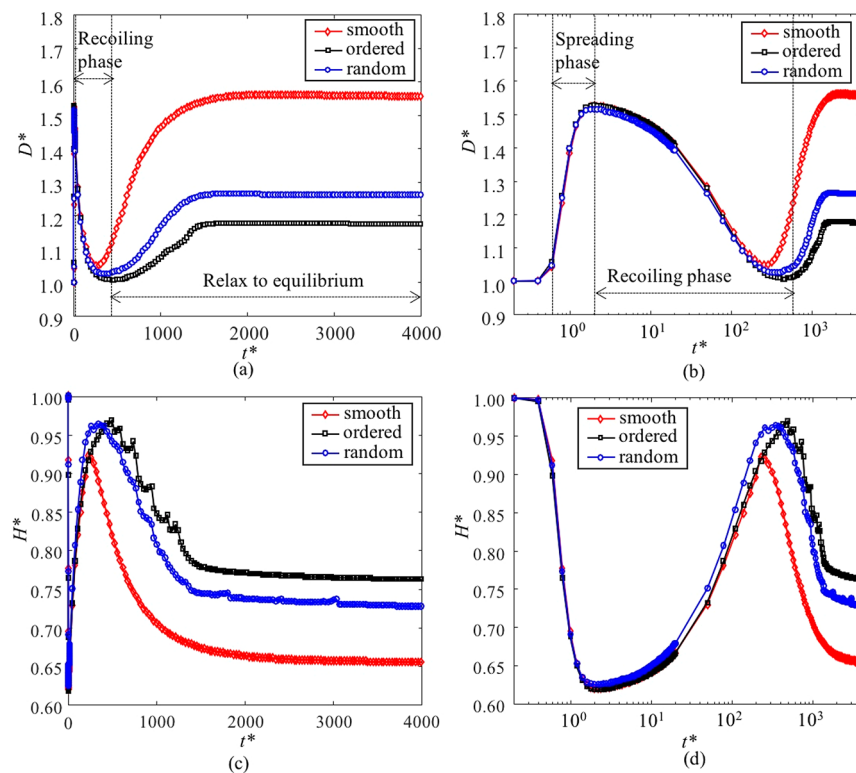


Figure 3. Droplet impact dynamics on smooth, rectangle, and randomly rough surfaces: (a and b) evolution of the spreading ratio D^* with dimensionless time; (c and d) evolution of the height ratio H^* with dimensionless time. The logarithmic scale is used for t^* in (b) and (d) to clearly show the behavior in the spreading and recoiling phases. Droplet diameter is $30 \mu\text{m}$; $R_r = 0.5 \mu\text{m}$ and $W_r = 1.8$ for two rough surfaces. Data for the randomly rough surface are average values based on five simulation runs.

shows that the VOF method significantly underestimated the oscillation magnitude after $t^* = 10$ and hence the time to reach an equilibrium state, while the model in this work could successfully capture the oscillation behavior in this stage. Note that reliable prediction of oscillation time to reach a final equilibrium state is especially important for a future study on coating formation by deposition of a huge amount of droplets. Impact of a new droplet on an oscillating droplet will be significantly different from the case of impact on a droplet at rest. In Case 2, a $40.9 \mu\text{m}$ droplet impacts on a surface with a contact angle of 88° (see property values listed in Table 1). The impact velocity is 2.21 m/s . As shown in Figure 2(b), predictions of spreading ratio dynamics capture well the trend of the experimental data taken from Dong et al. (2007).¹⁵ This phase field model has therefore been extended to explore the dynamics of droplet impact on randomly rough surfaces which have limited mentions in the literature.

3. RESULTS AND DISCUSSION

Although the numerical method introduced in the previous section is general and should be applicable to a wide range of droplets with different sizes and properties, this work focused on paint droplet deposition for coating formation. The size of the simulation domain is $Lx \times Ly = 120 \mu\text{m} \times 60 \mu\text{m}$. The initial droplet diameter (D_0) is $30 \mu\text{m}$, and it is placed $25 \mu\text{m}$ above the rough surface (see Figure 1(b)). The density and viscosity of the paint droplet are, respectively, $1,140 \text{ kg/m}^3$ and $0.15 \text{ Pa}\cdot\text{s}$. The surface tension is 0.02 N/m . The apparent contact angle of the droplet on a smooth surface is 80° (see Table 1). Furthermore, an additional volume force F_{set} (N/m^3) was exerted on the droplet in order to achieve the impact velocity of 15 m/s . It offers a Weber number of about 385. Once the droplet touched the

surface with the prespecified impact velocity, this additional force was taken away.

Numerical simulation was conducted to explore the dynamics of paint droplet impaction on surfaces with different morphologies. The model results of the droplet impact dynamics on smooth, patterned, and randomly rough surfaces are compared to demonstrate the influence of the surface morphology on the droplet impact behavior.

3.1. Comparison among Randomly Rough, Patterned, and Smooth Surfaces. After landing on a solid surface, a droplet may spread out, recoil, and relax to rest. The impact dynamics depend on the materials properties of both droplet and substrate, as well as surface morphology. It is known that droplet shape evolves on a rough surface quite differently as compared with the case on a smooth surface. As mentioned in the Introduction, various efforts focused on droplet impact on surfaces with ordered patterns (i.e., ordered rough surfaces). Can the droplet impact behavior on an ordered rough surface be adopted directly to characterize the impact case on a randomly rough surface? Or in other words, is there a need to investigate droplet impact on a randomly rough surface, which is the most common surface but is rarely studied in the open literature. In order to answer this question, three surfaces were considered in this work, i.e., smooth, rectangular patterned, and randomly rough surfaces. To ensure a fair comparison, two rough surfaces are set to have the same root-mean-square roughness and Wenzel roughness ratio (i.e., $R_r = 0.5 \mu\text{m}$ and $W_r = 1.8$).

As captured in Figure 3, the droplet impact dynamics on the three surfaces exhibit some similar characteristics. Under the specified conditions, the droplets experience three phases, the spreading phase, the recoiling phase, and the relaxation phase to

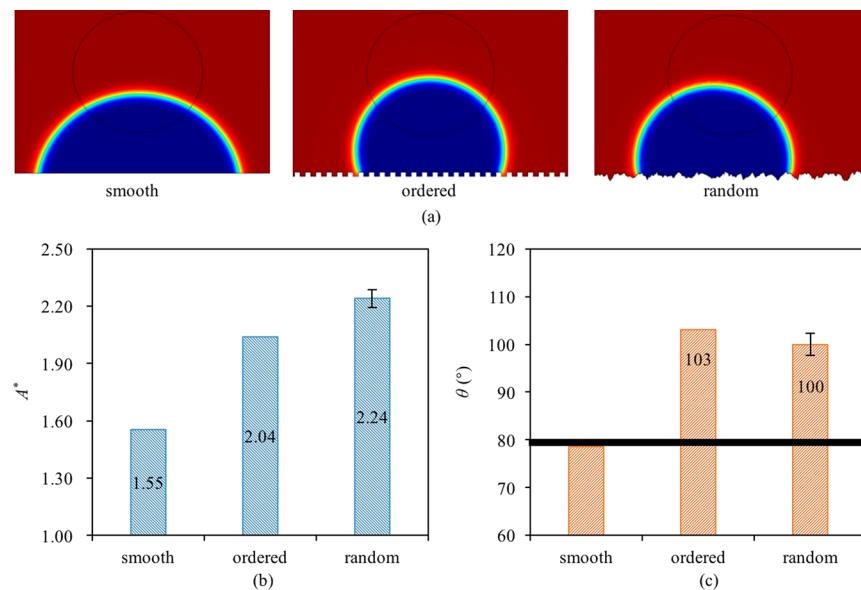


Figure 4. Comparison of equilibrium states: (a) the equilibrium state of a droplet respectively on the smooth, rectangle patterned, and randomly rough surfaces; (b) the equilibrium contact area; and (c) the equilibrium contact angle. Droplet diameter is $30\ \mu\text{m}$; $R_r = 0.5\ \mu\text{m}$ and $W_r = 1.8$ for two rough surfaces. For the randomly rough surface, average values and standard deviations of the equilibrium contact area and the equilibrium contact angle based on five simulation runs are plotted.

reach an equilibrium state. On reaching the horizontal solid surface, the droplet spreads out initially on the surface until a maximum spread is reached with the range of spreading and height ratios, $D^* \in [1, 1.527]$ and $H^* \in [0.618, 1]$, respectively. Shortly after spreading, the droplet retracts under the action of surface tension to the recoiling phase. The height of the droplet increases gradually and the spreading ratio decreases simultaneously at this stage. After that, the droplet relaxes to reach an equilibrium state. The spreading, recoiling, and relaxation phases last, respectively, around 2, 600, and 1000 in dimensionless time. To obtain a clear view of the spreading behavior, spreading and height ratios versus the dimensionless time plots at the logarithmic scale have been given in Figures 3(b) and 3(d), respectively. In all the cases investigated, the maximum spreading ratio and the minimum height ratio are, respectively, ~ 1.55 and ~ 0.62 . Figures 3(b) and 3(d) show that droplets on three surfaces demonstrate almost the same dynamics in the initial spreading phase. The time to reach the maximum spread is the same for three cases as well, i.e., $t^* = \sim 2$. These findings suggest that the initial spreading phase depends more on the kinetic energy of the droplet on impact rather than the surface morphology.

It is interesting to note the significant difference in spreading and height ratios among the surfaces from the recoiling phase onward. The droplet on the smooth surface exhibits the largest D^* and smallest H^* values. It suggests that the rough surfaces tend to promote recoil of the droplet (see the lower D^* and higher H^* values during the recoiling phase). This promotion effect is more significant for the ordered surface than the randomly rough surface. Furthermore, the droplet on the rectangular patterned surface achieves the minimum equilibrium spreading ratio compared to the randomly rough and smooth surfaces.

The difference of the equilibrium state have been further investigated. Figure 4 compares the equilibrium contact area as well as the equilibrium contact angle obtained for the three surfaces using eqs 12 and 13, respectively. Figure 4(a) gives the

topology of two rough surfaces having the same roughness. Droplets fully wet the surface, indicating a Wenzel state. The contact area of droplets on the rectangular patterned surface is smaller than the area on the randomly rough surface, while the droplet on the smooth surface has the smallest contact area (see Figure 4(b)). Meanwhile, droplets on rough surfaces have equilibrium contact angles higher than 80° (see Figure 4(c)). It is worthwhile to point out that the identified increasing trend is contradictory to the Wenzel theory and this contradiction seems more significant for the ordered surface than the randomly rough surface. According to the classical Wenzel theory, increasing the roughness of a hydrophilic surface can lead to the decrease of the contact angle (i.e., a more hydrophilic surface). But for the case in this work, two rough surfaces become hydrophobic instead. Experimental investigations by Jung and Bhushan also found that the contact angles on rough surfaces were greater than 90° when those for smooth surfaces were less than 90° .¹¹ The same contradiction to the Wenzel theory was also reported by Kang and Jacobi.⁵ It is interesting to note that in our modeling work and Jung and Bhushan's experimental work, the ratio between the droplet diameter and the surface roughness has a similar value, i.e., ~ 60 . This finding implies that the validity of the Wenzel theory may depend on the size difference between the droplet and the surface roughness. As shown in Figure 4(a), the pinning effect seems to play a role in the observed contact angles on rough surfaces. When the ratio between the droplet diameter and the surface roughness is small, the pinning effect of wetting on the rough surface may lead to the deviation from the Wenzel theory.³⁷ It will be interesting to carry out further investigations on the mechanisms leading to the contradiction to the Wenzel theory. But this is out of the scope of the current work.

The comparison results in this section show that droplet impact dynamics on a patterned surface cannot be directly used to represent droplet impact behavior on a randomly rough surface even if two types of surfaces have the same roughness. Although the difference of the maximum spreading ratios is

Table 2. Roughness of Randomly Rough Surfaces under Investigation

Surface roughness	Case 1	Case 2	Case 3	Case 4	Case 5	Case 6	Case 7	Case 8	Case 9
R_r (μm)	0.5	0.5	0.5	0.5	0.5	0.3	0.4	0.6	0.7
W_r	1.4	1.6	1.8	2.0	2.2	1.8	1.8	1.8	1.8

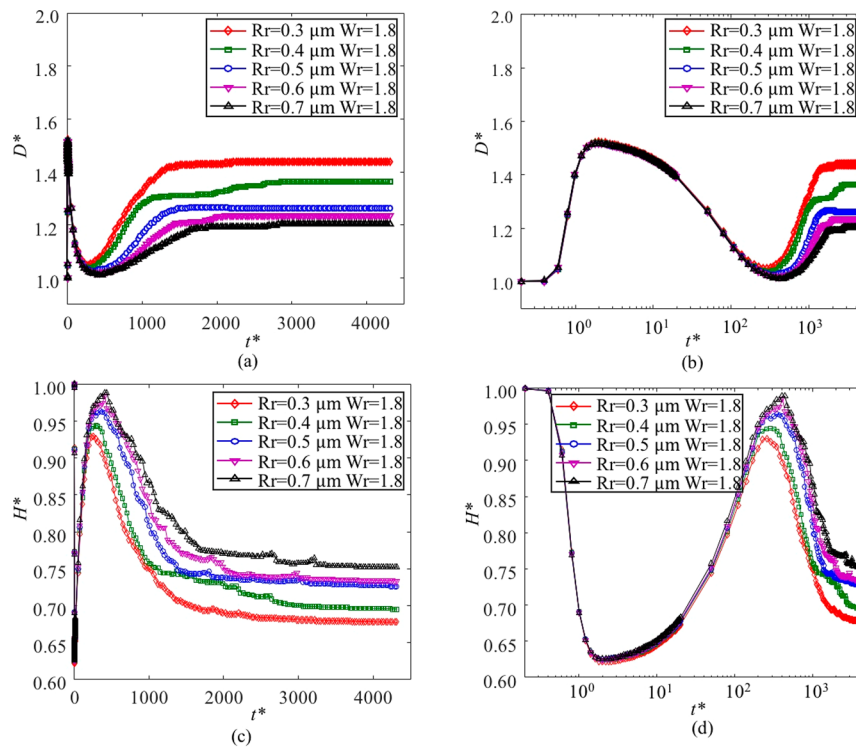


Figure 5. Droplet impact dynamics on surfaces having different values of the root-mean-square roughness but the same Wenzel roughness: (a and b) evolution of the spreading ratio D^* with dimensionless time; (c and d) evolution of the height ratio H^* with dimensionless time. The logarithmic scale is used for t^* in (b) and (d) to clearly show the behavior in the spreading and recoiling phases.

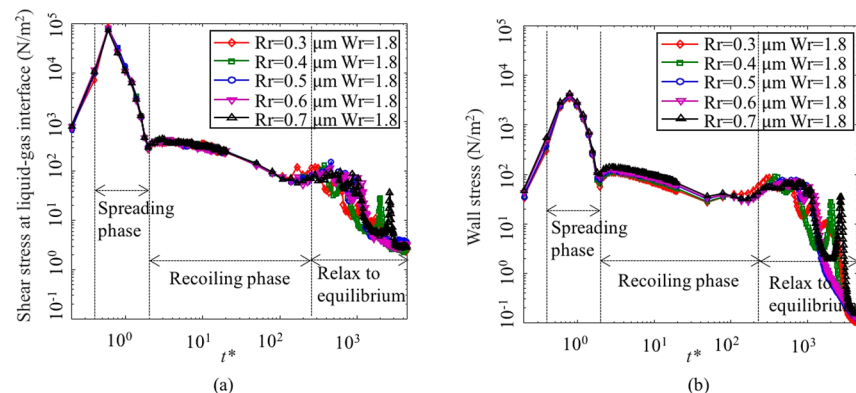


Figure 6. Shear stress evolution during droplet deposition on surfaces having different values of the root-mean-square roughness but the same Wenzel roughness: (a) average shear stress at the liquid–gas interface, and (b) average shear stress exerted by the fluid on the rough surface.

negligible, the droplets on two surfaces exhibit different behaviors in the recoiling and relaxation phases.

3.2. Effects of Varying Root-Mean-Square Roughness on Droplet Impact Dynamics. Eight randomly rough surfaces are further investigated to explore the effects of surface roughness on droplet impact dynamics. Five simulations with different droplet impact locations shown in Figure 1(a) are carried out for each surface. As shown in Table 2, two sets of surfaces are designed. The first set has the same R_r but different W_r values (Cases 1 to 5), while the second set has varying R_r values but the

same W_r (Case 3, Cases 6 to 9). Case 3 is the base case discussed in the last section. This design allows us to investigate the effects of two types of roughness independently.

Figures 5–7 demonstrate droplet impact dynamics on the second set of surfaces. As shown in Figure 5, the change of the root-mean-square roughness R_r has a negligible influence on the initial stage of droplet spreading. The maximum spreading and height ratios of the five investigated scenarios have the same values. It should be pointed out that both the surface morphology and the wetting state affect viscous dissipation during droplet

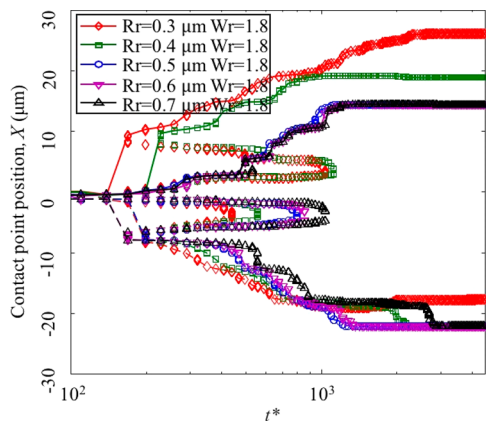


Figure 7. Evolution of the triple-phase (solid–liquid–gas) contact line, i.e., the position of triple-phase contact points in 2D. Horizontal positions are plotted. At a certain time, more than two contact points on a rough surface may exist. The rightmost contact points (RMCP) are connected using solid lines and the leftmost contact points (LMCP) are connected by dashed lines.

deposition. At the Wenzel state, a droplet fully wets the surface, and hence the influence from the surface morphology on viscous dissipation can be significant. However, this is not the case for the Cassie wetting state, where a droplet sits on the top of a textured surface with air pockets underneath. In this work, during the initial spreading phase, the Cassie state can be observed for cases with different surface morphologies (see Figure 8(a)). Thus, droplet shape evolution during this phase mainly depends on the impact velocity (i.e., the kinetic energy) rather than the surface morphology. Due to the deceleration from a high impact velocity, the initial spreading phase is associated with high shear stress at the liquid–gas interface. The fluid also exerts high shear stress on

the rough wall (Figure 6). There are no triple-phase contact points during this stage (see Figure 7), which confirms a Cassie wetting state.

As soon as the droplet retracts to the recoiling phase, the difference in R_r begins to define the magnitude of spreading. Droplet impacting the surface with the highest R_r value has the lowest and highest values of the spreading and height ratios, respectively (see Figures 5(b) and 5(d)). The shear stresses during the recoiling phase are lower than those of the initial spreading phase (Figure 6). Wetting of the rough surface starts at around $t^* = 100$ (see Figure 7), which is in the recoiling phase. After that, the distance between the rightmost contact point (RMCP) and the leftmost contact point (LMCP) begins to increase, implying the increasing trend of the liquid–solid contact area. At a certain time, more than two contact points can be identified, which indicates a transition wetting state between the Cassie and Wenzel states. After the recoiling phase, the droplets spread out again to reach an equilibrium state. Transition from the Cassie state to the Wenzel state continues, and thus the influence of surface morphology on the viscous dissipation becomes significant. After around 1000 (dimensionless time), only two contact points can be identified (Figure 7), indicating a fully wetted Wenzel state. As shown in Figure 6(b), increasing R_r leads to the increase of wall stress during the recoiling and relaxation stages and hence more viscous dissipation. This may explain the lower equilibrium spreading ratio of a droplet on a surface with a higher R_r value (Figure 5).

Figure 8 compares in detail the equilibrium states on five surfaces. All droplets are in the Wenzel state (Figure 8(a)). An inverse relationship can be observed between R_r and the equilibrium contact area. Increasing R_r value results in a decreasing equilibrium contact area. Specifically, the equilibrium contact area decreases linearly from around 2.59 to 2.13

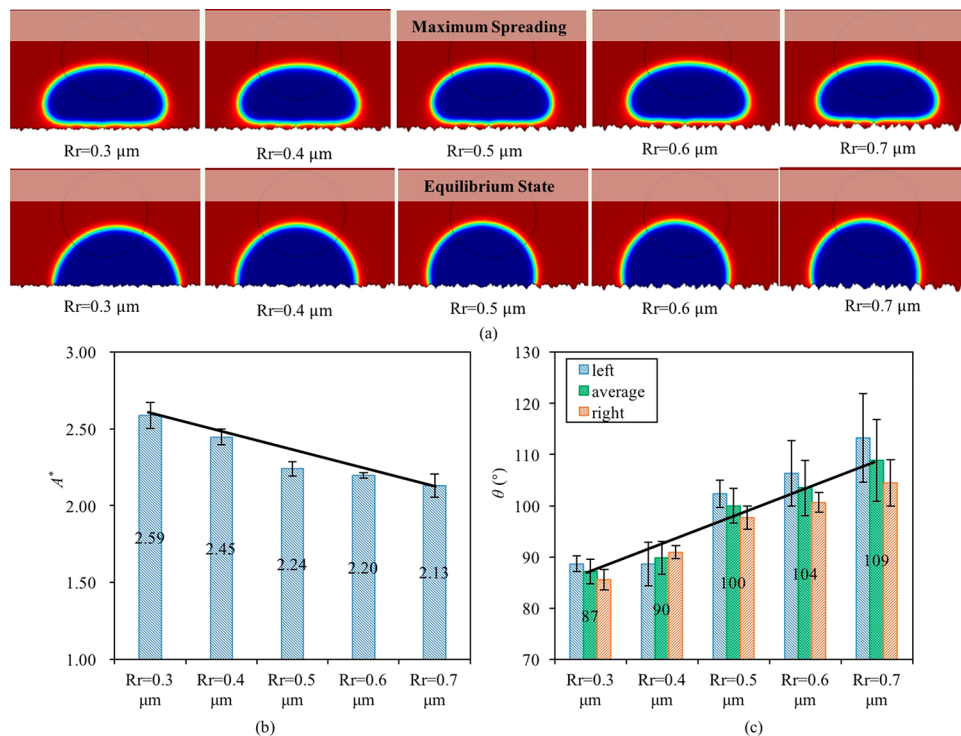


Figure 8. Comparison of equilibrium states of droplets on the randomly rough surfaces with the same value of $W_r = 1.8$ and different R_r ranging from 0.3 to 0.7 μm : (a) the maximum spreading and equilibrium states, (b) the equilibrium contact area, and (c) the equilibrium contact angle.

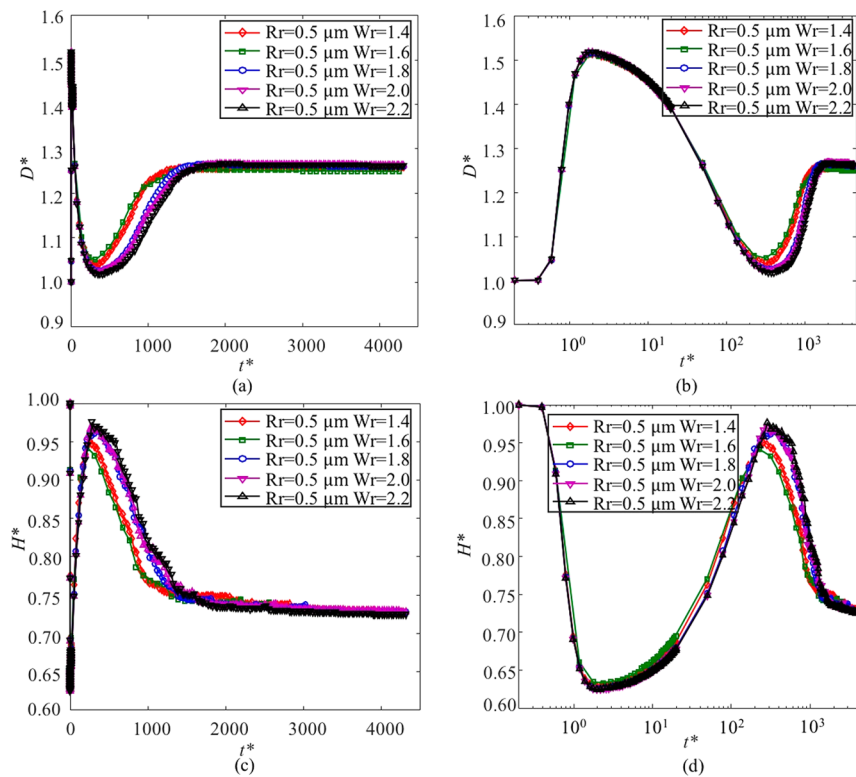


Figure 9. Droplet impact dynamics on surfaces having different values of the Wenzel roughness but the same root-mean-square roughness: (a and b) evolution of the spreading ratio D^* with dimensionless time, (c and d) evolution of the height ratio H^* with dimensionless time. The logarithmic scale is used for t^* in (b) and (d) to clearly show the behavior in the spreading and recoiling phases.

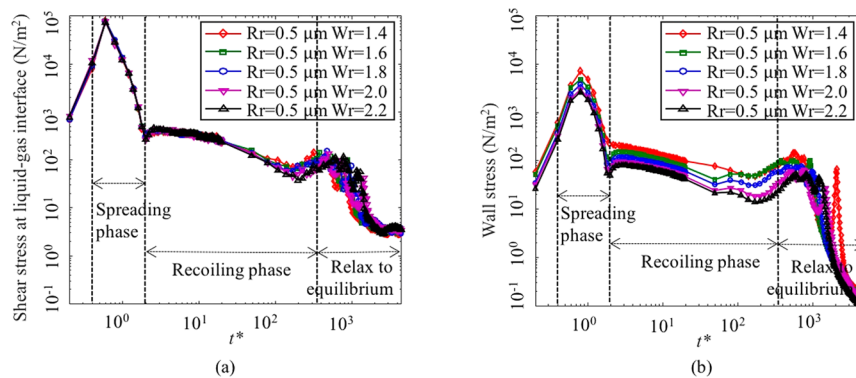


Figure 10. Shear stress evolution during droplet deposition on surfaces having different values of the Wenzel roughness but the same root-mean-square roughness: (a) average shear stress at the liquid–gas interface, and (b) average shear stress exerted by the fluid on the rough surface.

corresponding to R_r of 0.3 and 0.7 μm , respectively (Figure 8(b)). The triple-phase contact points plotted in Figure 7 confirm this trend as well. The average equilibrium contact angle increases from 87° to 109° with increasing R_r from 0.3 to 0.7 μm (see Figure 8(c)). The lowest average equilibrium contact angle (87°) corresponds to the surface with the lowest R_r value of 0.3 μm . Deviation from the Wenzel theory is least significant for this case. The ratio between the droplet diameter and the surface roughness for this case has the largest value (i.e., 100) in five cases, implying that large size difference between the droplet and the surface roughness may be the prerequisite for using the Wenzel theory to characterize the wetting behavior of rough surfaces.

3.3. Effects of Varying Wenzel Roughness on Droplet Impact Dynamics.

In order to investigate the effects of Wenzel roughness W_r on droplet impact dynamics, the root-mean-square

roughness R_r was kept constant while various cases of W_r were considered. Numerical results for changing W_r from 1.4 to 2.2 with R_r fixed at 0.5 μm are shown in Figures 9–12. As can be observed, the initial maximum spreading and height ratios of the five investigated scenarios have the same values with negligible influence of surface roughness at the initial stage of spreading (Figures 9(b) and 9(d)). Again, this phenomenon can be attributed to the Cassie wetting state during the initial spreading phase (Figure 12(a)). The shear stresses during the initial spreading phase are higher than those during the recoiling phase (Figure 10). Despite the variation in the surface Wenzel roughness, the spreading and height ratios of droplets keep close range as it retracts to the recoiling phase, which eventually leads to very identical D^* as well as H^* values for all W_r parameters at the equilibrium stage of the droplet (see Figures 9(a) and 9(c)). The Wenzel roughness, however, has clear

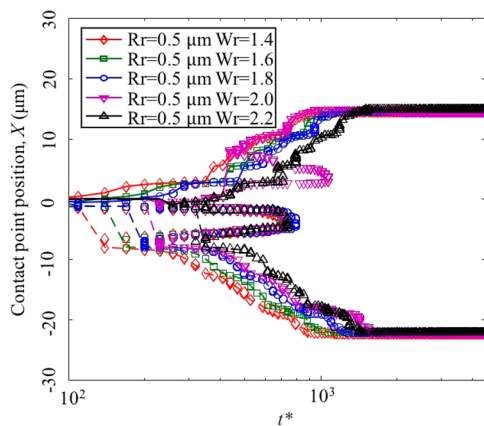


Figure 11. Evolution of the triple-phase (solid–liquid–gas) contact line, i.e., the position of triple-phase contact points in 2D. Horizontal positions are plotted. At a certain time, more than two contact points on a rough surface may exist. The rightmost contact points (RMCP) are connected using solid lines, and the leftmost contact points (LMCP) are connected by dashed lines.

influence on the time to reach the equilibrium state. It is interesting to note that the droplet on a surface with a lower W_r value needs less time to relax to an equilibrium state (see Figures 9 and 11). The higher wall stress (i.e., higher viscous dissipation) during the deposition process on a surface with a less W_r value may explain this phenomenon (Figure 10).

The equilibrium states are compared in Figure 12. Again, all droplets exhibit a wetting behavior of the Wenzel state (Figure 12(a)). Although all five cases have the same spreading ratio (see the value of D^* in Figure 9) and the same distance between RMCP and LMCP (Figure 11), droplets have different contact area with five surfaces. The equilibrium contact area increases linearly from 1.87 to 2.78 when the Wenzel roughness is

increased from 1.4 to 2.2 (Figure 12(b)). The change in average equilibrium contact angle for the same W_r is within 8° (Figure 12(c)). Increasing W_r , a weak increasing trend of the contact angle can be observed. Comparing Figure 8 and Figure 12, the results suggest that increasing different roughness values can even lead to the opposite effect on the equilibrium contact area. Again, numerical simulations allowed us to explore such distinctive effects of different roughness parameters on droplets' impact behavior and equilibrium states, which is a unique contribution of the current work.

4. CONCLUSIONS

In this work, a phase field model has been introduced to simulate the impact process of a single droplet on randomly rough surfaces. Comparisons were carried out between the rectangular patterned surface and the randomly rough surface. Results clearly show that even if two surfaces have the same roughness, the impact dynamics and equilibrium states of the droplet can be quite different. Specifically, the recoiling behavior of the droplet on the ordered surface is more significant. Moreover, at the equilibrium state, the droplet on the randomly rough surface demonstrates a larger spreading ratio and a lower contact angle. This observation justified the necessity for a systematic study of droplet impact on randomly rough surfaces, which can be hardly identified in the current open literature.

The model based simulation has revealed the interesting effects of two key morphological metrics (i.e., the Wenzel roughness parameter (W_r) and the root-mean-square roughness (R_r)) of a randomly rough surface on droplet impact behavior. The phenomena are summarized as follows. First, the surface roughness could barely affect the initial spreading phase of the droplet. The maximum spreading ratio was kept constant regardless of the values of W_r and R_r . At the equilibrium state, increasing R_r resulted in a reduction in both spreading ratio and contact area but an increase of the contact angle. Furthermore,

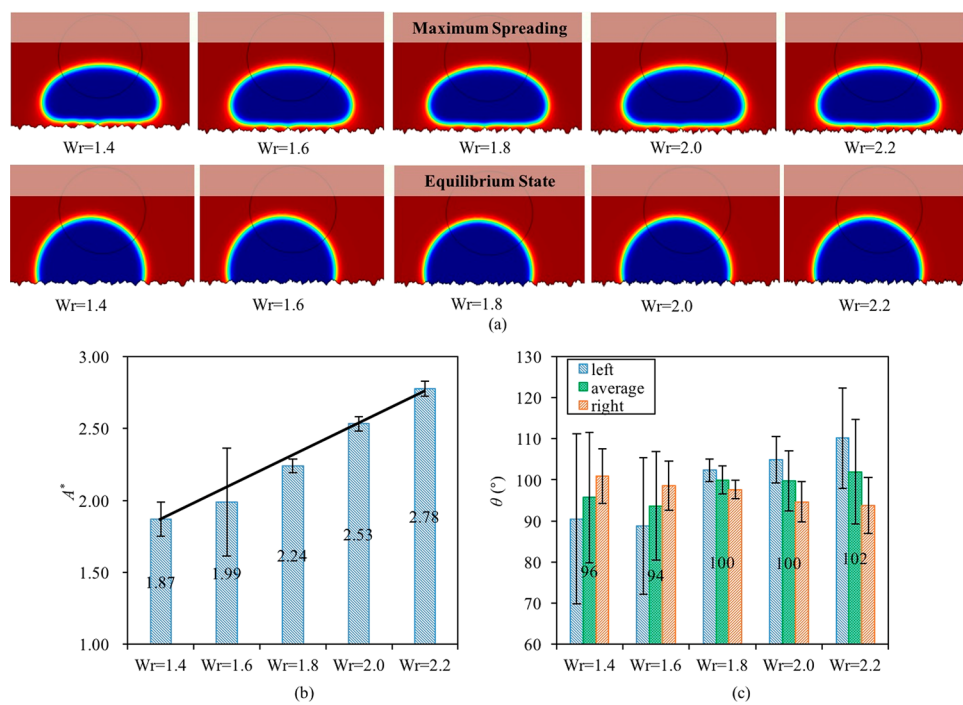


Figure 12. Comparison of equilibrium states of droplets on the randomly rough surfaces with the same value of $R_r = 0.5 \mu\text{m}$ and different W_r ranging from 1.4 to 2.2: (a) the maximum spreading and equilibrium states, (b) the equilibrium contact area, and (c) the equilibrium contact angle.

increasing the Wenzel roughness, W_r , took the droplet longer time to reach an equilibrium state. At the equilibrium state, increasing W_r resulted in an increase of the contact area and a slight increase of the contact angle. The equilibrium spreading ratio was not a function of the value of W_r . Finally, the ratio between the droplet size and the surface roughness may be one important parameter that affects the validity of the Wenzel theory.

The droplet investigated in this work is the Newtonian fluid. In practical applications, many fluids exhibit complex Non-Newtonian behavior. Our future work will extend this research to include non-Newtonian fluids. Although a validated 2D model is currently a decent option to uncover randomly rough surfaces' geometric effects on droplet impact dynamics with reasonable computational efficiency, a 3D model needs to be developed in the future to take care of the randomly rough surfaces in 3D. This work has also built a basis for a future study on the complex process of wet film formation, where deposition of a huge amount of droplets will be involved.

AUTHOR INFORMATION

Corresponding Author

*E-mail: jie.xiao@suda.edu.cn.

ORCID

Jie Xiao: [0000-0001-7842-7862](https://orcid.org/0000-0001-7842-7862)

Yinlun Huang: [0000-0001-8370-6268](https://orcid.org/0000-0001-8370-6268)

Notes

The authors declare no competing financial interest.

ACKNOWLEDGMENTS

We are grateful for the financial support from the National Natural Science Foundation of China (21406148), the Natural Science Foundation of Jiangsu Province (BK20170062), the "Jiangsu Innovation and Entrepreneurship (Shuang Chuang) Program", the "Jiangsu Specially-Appointed Professors Program", and the "Priority Academic Program Development (PAPD) of Jiangsu Higher Education Institutions".

NOMENCLATURE

A^* = dimensionless liquid–solid contact area

D = furthest horizontal distances between droplet surface points (m)

D_0 = droplet initial diameter (m)

D^* = spreading ratio

E_{mix} = mixing energy (J/m^3)

F = volume force vector (N/m^3)

\vec{g} = gravity vector (m/s^2)

G = chemical potential (J/m^3)

h_i = height of the data point (m)

\bar{h} = mean height of all n data points (m)

H = furthest vertical distances between droplet surface points (m)

H^* = height ratio

l = length of the liquid–solid contact line (m)

p = pressure (Pa)

R_e = Reynolds number

R_r = root-mean-square roughness

t = time (s)

t^* = dimensionless time

\vec{V} = velocity vector (m/s)

V_0 = velocity of impact (m/s)

W_e = Weber number

W_r = Wenzel roughness

Greek Letters

α = volume fraction

β = mobility ($m^3 \cdot s/kg$)

ϵ = interface thickness (m)

θ = contact angle (deg)

λ = mixing energy density (N)

ρ = density (kg/m^3)

σ = surface tension (N/m)

ϕ = dimensionless phase-field parameter

Ω = domain

Subscripts

1 = left

2 = right

a = air

w = liquid

REFERENCES

- (1) Xiao, J.; Li, J.; Piluso, C.; Huang, Y. L. Multiscale characterization of automotive surface coating formation for sustainable manufacturing. *Chin. J. Chem. Eng.* **2008**, *16*, 416–423.
- (2) Li, J.; Xiao, J.; Huang, Y. L.; Lou, H. H. Integrated process and product analysis: a multiscale approach to paint spray. *AIChE J.* **2007**, *53*, 2841–2857.
- (3) Xiao, J.; Li, J.; Lou, H. H.; Xu, Q.; Huang, Y. L. ACS-based dynamic optimization for curing of polymeric coating. *AIChE J.* **2006**, *52*, 1410–1422.
- (4) Peters, C. A.; Nichols, M. E.; Ellwood, K. R. J. The evolution of surface texture in automotive coatings. *Journal of Coatings Technology and Research* **2011**, *8*, 469–480.
- (5) Kang, H. C.; Jacobi, A. M. Equilibrium contact angles of liquid droplets on ideal rough solids. *Langmuir* **2011**, *27*, 14910–14918.
- (6) Zhang, B.; Wang, J.; Liu, Z.; Zhang, X. Beyond Cassie equation: Local structure of heterogeneous surfaces determines the contact angle of microdroplets. *Sci. Rep.* **2015**, *4*, 1–7.
- (7) Swain, P. S.; Lipowsky, R. Contact angles on heterogeneous surfaces: a new look at Cassie's and Wenzel's Laws. *Langmuir* **1998**, *14*, 6772–6780.
- (8) Wolansky, G.; Marmur, A. Apparent contact angles on rough surfaces: the Wenzel equation revisited. *Colloids Surf., A* **1999**, *156*, 381–388.
- (9) Whyman, G.; Bormashenko, E.; Stein, T. The rigorous derivation of Young, Cassie-Baxter and Wenzel equations and the analysis of the contact angle hysteresis phenomenon. *Chem. Phys. Lett.* **2008**, *450*, 355–359.
- (10) He, B.; Patankar, N. A.; Lee, J. Multiple equilibrium droplet shapes and design criterion for rough hydrophobic surfaces. *Langmuir* **2003**, *19*, 4999–5003.
- (11) Jung, Y. C.; Bhushan, B. Wetting behavior of water and oil droplets in three-phase interfaces for hydrophobicity/phobicity and oleophobicity/phobicity. *Langmuir* **2009**, *25*, 14165–14173.
- (12) Kwon, Y.; Patankar, N.; Choi, J.; Lee, J. Design of surface hierarchy for extreme hydrophobicity. *Langmuir* **2009**, *25*, 6129–6136.
- (13) Wong, T.; Sun, T.; Feng, L.; Aizenberg, J. Interfacial materials with special wettability. *MRS Bull.* **2013**, *38*, 366–371.
- (14) Tian, Y.; Su, B.; Jiang, L. Interfacial material system exhibiting superwettability. *Adv. Mater.* **2014**, *26*, 6872–6897.
- (15) Dong, H.; Carr, W. W.; Bucknall, D. G.; Morris, J. F. Temporally-resolved inkjet drop impaction on surfaces. *AIChE J.* **2007**, *53*, 2606–2617.
- (16) Scheller, B. L.; Bousfield, D. W. Newtonian drop impact with a solid surface. *AIChE J.* **1995**, *41*, 1357–1367.
- (17) Mao, T.; Kuhn, D. C. S.; Tran, H. Spread and rebound of liquid droplets upon impact on flat surfaces. *AIChE J.* **1997**, *43*, 2169–2179.
- (18) Gao, X.; Li, R. Spread and recoiling of liquid droplets impacting solid surfaces. *AIChE J.* **2014**, *60*, 2683–2691.

- (19) Gunjal, P. R.; Ranade, V. V.; Chaudhuri, R. V. Dynamics of drop impact on solid surfaces: experiments and VOF simulations. *AIChE J.* **2005**, *51*, 59–78.
- (20) Zhou, W.; Loney, D.; Degertekin, F. L.; Rosen, D. W. What controls dynamics of droplet shape evolution upon impingement on a solid surface? *AIChE J.* **2013**, *59*, 3071–3082.
- (21) Zhang, D.; Papadikis, K.; Gu, S. Application of a high density ratio lattice-Boltzmann model for the droplet impingement on flat and spherical surfaces. *Int. J. Therm. Sci.* **2014**, *84*, 75–85.
- (22) Li, X.; Mao, L.; Ma, X. Dynamic behavior of water droplet impact on microstructured surfaces: the effect of geometrical parameters on anisotropic wetting and the maximum spreading diameter. *Langmuir* **2013**, *29*, 1129–1138.
- (23) Dupuis, A.; Yeomans, J. M. Modeling droplets on superhydrophobic surfaces: equilibrium states and transitions. *Langmuir* **2005**, *21*, 2624–2629.
- (24) Kusumaatmaja, H.; Yeomans, J. M. Modeling contact angle hysteresis on chemically patterned and superhydrophobic surfaces. *Langmuir* **2007**, *23*, 6019–6032.
- (25) Kusumaatmaja, H.; Vrancken, R. J.; Bastiaansen, C. W. M.; Yeomans, J. M. Anisotropic drop morphologies on corrugated surfaces. *Langmuir* **2008**, *24*, 7299–7308.
- (26) David, R.; Neumann, W. Contact angle hysteresis on randomly rough surfaces: a computational study. *Langmuir* **2013**, *29*, 4551–4558.
- (27) Yuan, W. Z.; Zhang, L. Z. Lattice Boltzmann simulation of droplets impacting on super-hydrophobic surfaces with randomly distributed rough structures. *Langmuir* **2017**, *33*, 820–829.
- (28) Meiron, T. S.; Marmur, A.; Saguy, I. S. Contact angle measurement on rough surfaces. *J. Colloid Interface Sci.* **2004**, *274* (2), 637–44.
- (29) Stow, C. D.; Hadfield, M. G. An Experimental Investigation of Fluid Flow Resulting from the Impact of a Water Drop with an Unyielding Dry Surface. *Proc. R. Soc. London, Ser. A* **1981**, *373* (1755), 419–441.
- (30) Shiri, S.; Bird, J. C. Heat exchange between a bouncing drop and a superhydrophobic substrate. *Proc. Natl. Acad. Sci. U. S. A.* **2017**, *114*, 6930–6935.
- (31) Bernardin, J. D.; Stebbins, C. J.; Mudawar, I. Mapping of impact and heat transfer regimes of water drops impinging on a polished surface. *Int. J. Heat Mass Transfer* **1997**, *40*, 247–267.
- (32) Bertola, V. An impact regime map for water drops impacting on heated surfaces. *Int. J. Heat Mass Transfer* **2015**, *85*, 430–437.
- (33) Xiao, J.; Chaudhuri, S. Design of anti-icing coatings using supercooled droplets as nano-to-microscale probes. *Langmuir* **2012**, *28*, 4434–4446.
- (34) Yang, F.; Zheng, Z.; Xiao, R.; Shi, H. Comparison of two fractal interpolation methods. *Phys. A* **2017**, *469*, 563–571.
- (35) Izquierdo, S.; Lopez, C. I.; Valdes, J. R.; Miana, M.; Martinez, F. J.; Jimenez, M. A. Multiscale characterization of computational rough surfaces and their wear using self-affine principal profiles. *Wear* **2012**, *274–275*, 1–7.
- (36) COMSOL, A. B. *COMSOL Multiphysics User's Guide*; COMSOL AB: Sweden, 2008.
- (37) Kurogi, K.; Yan, H.; Tsujii, K. Importance of pinning effect of wetting in super water-repellent surfaces. *Colloids Surf., A* **2008**, *317*, 592–597.